Effect of temperature on lanthanide charge transition levels and vacuum referred binding energies

Dorenbos, Pieter

DOI
10.1016/j.jlumin.2024.120443

Publication date
2024

Document Version
Final published version

Published in
Journal of Luminescence

Journal of Luminescence 269 (2024) 120443

Contents lists available at ScienceDirect

Journal of Luminescence

journal homepage: www.elsevier.com/locate/jlumin

Full Length Article

Effect of temperature on lanthanide charge transition levels and vacuum referred binding energies

Pieter Dorenbos

Delft University of Technology, Faculty of Applied Sciences, Department of Radiation Science and Technology, Mekelweg 15, 2629 JB Delft, Netherlands

A B S T R A C T

Location of lanthanide levels in the bandgap, vacuum referred binding energy (VRBE) in the lanthanide ground state and energy of lanthanide charge transition levels (CTLs) are just three different namings for the same concept. A concept of importance for the performance of lanthanide activated compounds. Energy differences of CTLs with the conduction band bottom and valence band top are important when it concerns e.g. lanthanide luminescence, charge carrier trapping, and valence stability. Effect of temperature on CTL energy or VRBE has so far never been addressed despite that luminescence application and thermoluminescence studies may span a temperature range from 10 K to 1000 K. In this work information on the bandgap (or energy of host exciton creation) around 10 K and at RT in compounds is gathered to demonstrate that bandgap decreases by 0.1 eV to 0.3 eV when temperature increases to RT. A similar decrease will be demonstrated for the energy of electron transfer from the VB to a trivalent lanthanide. The findings have consequences for VRBE-diagram construction, i.e. the experimental parameters for such construction should all apply to the same temperature. They also have consequences on how to relate luminescence thermal quenching energy barriers and TL derived electron and hole trap depths with a VRBE diagram. By proper evaluating the effects of temperature, accuracy of VRBE diagrams and consistency with luminescence and thermoluminescence data can be improved.

1. Introduction

Knowledge on the location or energy of the lanthanide charge transition levels (CTLs) in any kind of chemical environment is important to understand or engineer phenomena involving charge carrier transfer in that environment. Some of the lanthanides may trap an electron from the conduction band (CB) as illustrated with arrow 1) in Fig. 1 for $Sm^{3+} + e^- \rightarrow Sm^{2+}$. Some lanthanide may trap a hole from the valence band (VB) as illustrated with arrow 2) in Fig. 1 for $Pr^{3+} + h^+ \rightarrow Pr^{4+}$. Such trapping phenomena are studied by thermoluminescence (TL) techniques [1,2], and the phenomena play a crucial role in e.g. dosimetry phosphors for radiation monitoring [3], storage phosphors for X-ray or optical imaging, persistent phosphors for glow in the dark applications as in emergency signalling [4], phosphors for anti-counterfeiting, mechano-luminescence for stress sensing, and in-vivo imaging [5]. Hole transfer from a lanthanide to the VB or electron transfer from a lanthanide to the conduction band is often responsible for thermal quenching of lanthanide luminescence [6].

It turns out that the variation in lanthanide CTL energy with increasing number of electrons in the 4f-orbital always follows characteristic zigzag patterns as illustrated with curves a) and b) in the vacuum referred binding energy diagram of Fig. 1. The most crucial parameter for constructing such diagram is the U-value for Eu which expresses, see arrow 3, the energy difference between the $Eu^{3+/2+}$ and $Eu^{4+/3+}$ CTLs. The U-value scales in a systematic thus predictable fashion with the properties of the chemical environment [7]. The 2012 Chemical Shift model established a relationship between the U-value and the $Eu^{3+/2+}$ CTL with respect to the vacuum level defined as our zero of energy [8]. To find the CTLs of the lanthanides other than Eu, the variation in the 3rd and 4th ionization potentials of the lanthanides is exploited. That variation is then modified in compounds by the lanthanide ionic radius contraction and the nephelauxetic effect. These modifications have been parameterized with the contraction tilt parameters $\alpha(2+)$ and $\alpha(3+)$ and the nephelauxetic parameters $\beta(2+)$ and $\beta(3+)$ [9,10]. Parameters that show a mild, yet predictable, dependence on type of compound or chemical environment. It turned out that the characteristic zigzag shapes are rather invariant with type of compound, and compound-to-compound variations remain limited to a few 0.1 eV. The reader is referred to Ref. [7–12] for further information on the theory and methods of VRBE determination and construction. By using the experimentally determined energy $E^{CT}(Eu^{3+})$ of the VB→Eu^{3+} charge transfer (CT) band (arrow 4) observed in excitation spectra of Eu^{3+} emission, the CTL or VRBE E_V at the top of the VB can be found. Adding the energy E^{ex} for host exciton creation (arrow 5) and the exciton electron-hole binding energy $E_{e-h} \approx 0.008 \times (E^{ex})^2$ (arrow 6) [13] one arrives at the VRBE E_C at the conduction band (CB) bottom.

E-mail address: p.dorenbos@tudelft.nl.

https://doi.org/10.1016/j.jlumin.2024.120443
Received 1 December 2023; Received in revised form 3 January 2024; Accepted 5 January 2024
Available online 9 January 2024

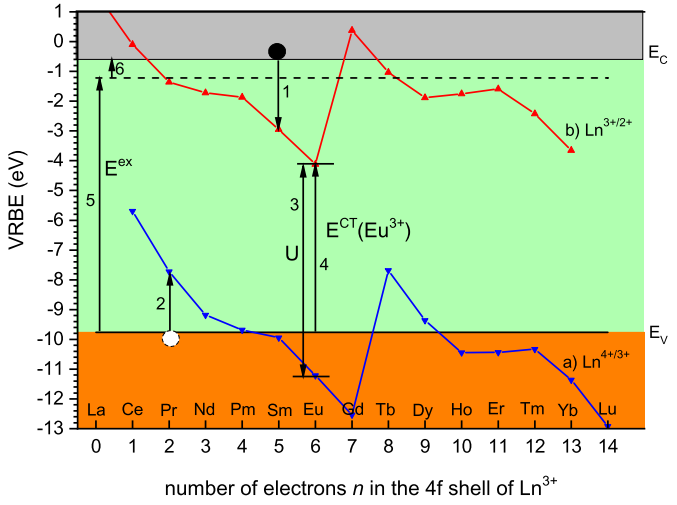

Fig. 1. Vacuum referred binding energy diagram with the location of the $Ln^{4+/3+}$ and $Ln^{3+/2+}$ charge transition levels connected with characteristic zigzag solid curves a) and b). The arrows indicate various charge carrier transitions that can be experimentally observed.

Note that in the above method for VRBE diagram construction, the effects of lattice relaxation that always takes place after charge carrier transfer are not accounted for. Furthermore, since first publication of the Chemical Shift model in 2012 [8,11] and later the Refined Chemical Shift model in 2019 [9,10], the effect of temperature on VRBE was always ignored. Temperature was at those times not regarded of much relevance considering the always present systematic errors in VRBE diagram construction and errors in the underlying main construction parameters U, $E^{CT}(Eu^{3+})$, and E^{ex}. For practical reasons the room temperature (RT) $E^{CT}(Eu^{3+})$ was used because the large majority of data in literature pertains to RT. For E^{ex} the value at 10 K was used because that appeared most accurate.

To test the accuracy and consistency of VRBE diagrams, information on the temperature of thermal quenching of lanthanide luminescence due to electron transfer from the emitting state to the CB or hole transfer from the emitting state to the VB can be used as was done in [6]. One may also use data from thermoluminescence glow peaks due to electron or hole release from a lanthanide to the CB or to the VB. Quenching temperature may vary from zero to 1000 K depending on type of compound and type of lanthanide, and within the same compound the maximum of a lanthanide related glow peak may vary from 100 K to 900 K as in YPO_4 [1,5,14,15]. To compare such data with a VRBE diagram we need to know how temperature affects the CTL energies of lanthanides and the CTL energies of E_V and E_C.

It is well established that the bandgap of inorganic and semiconductor compounds decreases when temperature increases at a rate that may vary from 0.3 to 0.8 meV/K [16,17]. This is caused by a combined effect of thermal lattice expansion and electron phonon interaction (EPI) [18]. Over a 100-1000 K temperature range then the bandgap may decrease by as much as 0.5 eV. In other words, the VB-top and CB-bottom move closer together and their CTLs have to shift several 0.1 eV. Clearly temperature needs to be considered in order to properly evaluate quenching energy barriers and trapping depths and to improve overall accuracy of VRBE diagram construction.

One may distinguish relative and absolute accuracy of lanthanide CTLs. Relative accuracy relates to the CTL energy difference between two different lanthanides, i.e., the shape of the $Ln^{3+/2+}$ and $Ln^{4+/3+}$ zigzag curves in Fig. 1. That accuracy is around 0.1 eV. Absolute accuracy relates to the error in VRBE of the entire zigzag curve and of E_V and E_C which may amount to 0.3-0.5 eV. That may seem quite large but is comparable with errors obtained with other methods like from ultraviolet photoelectron spectroscopy (UPS) [19], or from determination of flatband potentials using impedance measurement techniques [20], or from redox potentials in electrochemistry. By properly addressing the effect of temperature on the VRBE, the expectation is to improve accuracy of VRBE construction or otherwise to gain knowledge on the fundamental limitation of the chosen method of VRBE construction. It is the aim of this paper to address those issues.

2. Theory and methods

The Chemical Shift model is based on the phenomenon that a cation in a chemical environment (an ionic crystal, a glass, a liquid, a metal or an organic compound) always attracts negative charge as closely as possible in order to minimize the total energy of the 'system'. A Q+ cation will be screened by effectively Q- charge at a screening distance of R_{Q+}. The energy needed to remove an electron from such cation is then the ionisation energy of the free cation *reduced* by the Coulomb repulsion energy between an electron and the Q- negative screening charge at distance R_{Q+}. This reduction is called the chemical shift E^{cs} and is given by Coulomb's law

$$E^{cs}(Q+) = \frac{1440Q}{R_{Q+}} \quad (1)$$

where the screening distance is in pm and energy in eV. Similarly, one may argue that a $Q-$ anion will be screened by effectively $Q+$ charge at a screening distance of R_{Q-}. The energy needed to remove an electron from such anion is then the ionization energy of the free anion *augmented* by the Coulomb attraction between an electron and the positive screening charge. It causes a downward chemical shift of binding energy of magnitude

$$E^{cs}(Q-) = \frac{-1440Q}{R_{Q-}}. \quad (2)$$

Note that the wording ionization energy for anions like O^{2-} is somewhat a misnomer since as free ion it will spontaneously lose an electron and ionization energy is negative. Eq. (1) and Eq. (2) give a rather naive picture that concentrates all effects of bonding, ionicity, lattice structure, and lattice relaxation in just the screening lengths R_{Q+} and R_{Q-}. Although naive, it appears to provide a very good basis to organise and explain compound properties with a simple and intuitive model.

For Eu^{2+} (Q = 2) with $4f^7$ ground state electron configuration, the screening distance in inorganic compounds appears about 138 pm which is slightly larger than the 120 pm to 135 pm ionic radius reported for Eu^{2+} [21]. The upward chemical shift from the free ion $Eu^{3+/2+}$ CTL of -24.92 eV [8], which is equivalent to minus the 3rd ionization potential of Eu, is then 20.9 eV bringing the $Eu^{3+/2+}$ CTL near -4 eV as in Fig. 1. Compound to compound variation in screening distance, or chemical shift, or $Eu^{3+/2+}$ CTL depends on how strong electrons are bonded in the anions of a compound. Bonding is strongest in fluorine anions and R_{2+} will be longest (≈ 138 pm). Bonding is weakest in the pure lanthanide metals with free conduction band electrons and R_{2+} will be shortest (≈ 128 pm) [7,8].

For Eu^{3+} (Q = 3) with $4f^6$ ground state electron configuration, the chemical shift is about 3/2 larger than for Eu^{2+} because of the 3/2 larger screening charge. The $Eu^{4+/3+}$ CTL in compounds is then shifted from the free ion value of -42.97 eV [8] to values in the range -10 to -12 eV [7] as in Fig. 1. The energy difference between the $Eu^{3+/2+}$ and $Eu^{4+/3+}$ CTLs or the U-value ranges between 5.7 eV for the lanthanide metals up to 7.6 eV for the fluoride compounds [12]. It amounts 7.09 eV for the diagram in Fig. 1 which is a value typical for phosphate compounds. Methods to determine or estimate the U-value with about ±0.1 eV accuracy with as only information the composition of the compound can be found in Ref. [22].

The ionic radius of the lanthanides decreases by about 18 pm when moving through the lanthanide series from La to Lu [21]. Due to lattice relaxation, the screening distance will follow the decreasing ionic radius and the chemical shift will increase in going from La to Lu. This is the

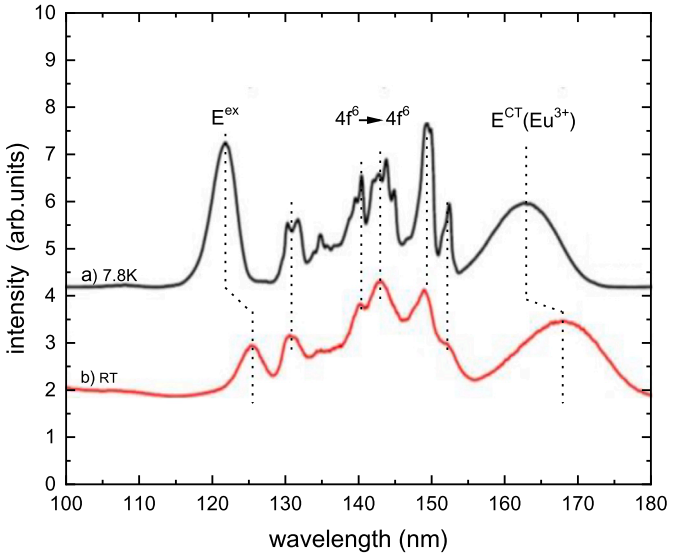

Fig. 2. Excitation spectra of 591 nm Eu^{3+} emission in Cs_2NaYF_6 obtained from Tanner et al. [23] with curve a) at 7.8 K and curve b) at 300 K. The exciton band E^{ex} and charge transfer band $E^{CT}(Eu^{3+})$ shift to longer wavelength when temperature increases but the intrinsic $4f^6 \rightarrow 4f^6$ excitation bands remain stationary.

origin of the tilting of the lanthanide CTL curves with respect to the free ion CTL curves and accounted for by the tilt parameters $\alpha(2+)$ and $\alpha(3+)$ in VRBE diagram construction.

3. Temperature dependence of E^{ex} and E^{CT}

The temperature dependence of exciton creation energy and the Eu^{3+} CT-band energy is nicely demonstrated with excitation spectra of Eu^{3+} luminescence in Cs_2NaYF_6 from the work of Tanner et al. [23]. Fig. 2 shows those spectra measured at 7.8 K and 300 K for the 591 nm Eu^{3+} emission. The exciton peak shifts from 121.6 nm at 7.8 K to 125.2 nm at RT corresponding with 0.29 eV decrease. The CT band at 161.4 nm shifts towards 166.4 nm corresponding with 0.23 eV. The narrow excitation lines between 128 nm and 152 nm corresponding with transitions to excited $4f^6$ states of Eu^{3+} remain stationary with temperature increase.

The temperature dependence of the bandgap of semiconductor compounds has been most widely studied, and tabulated data reveal [16,24] bandgap changes of 0.3-0.8 meV/K. In this work, a literature study is performed to obtain data on the band gap in wide bandgap (4 eV to 12 eV) compounds at temperature around liquid He and at room temperature (RT). The energy difference $E^{ex}(\approx 10\ K) - E^{ex}(RT)$ is shown against $E^{ex}(\approx 10\ K)$ in Fig. 3. The data with references can be found in Table 1. Occasionally literature provides E^{ex} at temperature other than 10 K, like 20 K for $LiCaAlF_6$ or 25 K for $KSrPO_4$. In those cases $E^{ex}(10K)$ was estimated from extrapolation.

Data show that E^{ex} increases with 0.1 to 0.3 eV when temperature increases from 10 K to RT which corresponds to 0.34 to 1.0 meV/K. There appears to be a trend that the increase scales with the size of E^{ex} as illustrated by the dashed line expressed by $0.07 + 0.021\ E^{ex}$. Fig. 3 also shows that for a fixed E^{ex} there can be quite large compound-to-compound variation, and there is even a negative value for $MgLa_2TiO_6$. It will be clear that with 0.1-0.3 eV change of E^{ex} between 10 K and RT one needs to construct a VRBE diagram at a specific temperature using parameters E^{ex}, E^{CT}, and U that apply to that temperature.

The effect of lattice expansion on the bandgap can be understood with the Chemical Shift model. When bondlengths increase due to lattice expansion, anions move further away from cations and the Coulomb repulsion between the negatively charged anion and a cation electron will reduce. One may equally well state that the screening distance R_{Q+} increases and chemical shift will reduce as expressed with Eq. (1). The CTL of a lanthanide (a cation) will then move down. The CB-bottom is dominantly formed by cation orbital states and therefore also E_C will move down. Increase of bondlengths implies also that the Coulomb attraction of the positive cations on the anion electrons will reduce as expressed with Eq. (2), and as a result the CTL of anions move upwards. The overall effect is a reduction of the band gap when temperature increases. Lattice expansion appears only partly responsible for bandgap

Table 1
The E^{ex} decrease between 10 K and room temperature together with the value for E^{ex} at 10 K. Energies are in eV.

Compound	E^{ex}(10 K)	E^{ex}(10 K)-E^{ex}(RT)	Ref.
InSb	0.2	0.07	[16]
InAs	0.4	0.08	[16]
Ge	0.7	0.12	[16]
GaSb	0.8	0.11	[16]
Si	1.2	0.09	[16]
InP	1.4	0.11	[16]
GaAs	1.5	0.13	[16]
CdTe	1.6	0.09	[16]
AlSb	1.7	0.09	[16]
CdSe	1.8	0.12	[16]
InN	2.0	0.06	[16]
AlAs	2.2	0.11	[16]
GaP	2.3	0.14	[16]
ZnTe	2.4	0.13	[16]
PbI_2	2.5	0.14	[36]
CdS	2.6	0.12	[16]
ZnSe	2.8	0.14	[16]
$Cs_3Bi_2I_8$	2.9	0.06	[37]
SiC	3.0	0.13	[16]
GaN	3.5	0.17	[16]
ZnS	3.8	0.10	[38]
$CaTiO_3$	3.8	0.02	[39,40]
ZnS	3.8	0.16	[16]
$LuVO_4$	3.9	0.15	[41,42]
$GdVO_4$	3.9	0.13	[41]
$MgLa_2TiO_6$	4.1	-0.07	[43]
KPb_2Cl_5	4.2	0.14	[44,45]
$KLuS_2$	4.2	0.15	[46]
$CaGa_2S_4$	4.4	0.22	[47]
ZnI_2	4.5	0.17	[48]
$CaWO_4$	4.8	0.16	[49]
Cs_2ZrCl_6	4.8	0.18	[50]
$LaSi_3N_5$	4.9	0.14	[51]
Lu_2O_3	5.3	0.10	[52]
$LiTaO_3$	5.4	0.18	[53]
C (diamond)	5.5	0.14	[16]
MgS	5.5	0.17	[54]
NaI	5.6	0.25	[55]
$SrZrO_3$	5.7	0.20	[56]
Cs_2HfCl_6	5.7	0.19	[57]
Y_2O_3	6.0	0.20	[58,59]
Sc_2O_3	6.1	0.25	[60]
AlN	6.2	0.24	[16]
Lu_2SiO_5	6.7	0.21	[61]
KBr	6.8	0.28	[17,62]
CsBr	6.8	0.31	[17,62]
Gd_2SiO_5	6.8	0.07	[63]
GdOCl	6.9	0.19	[64]
$Ba_2Mg(BO_3)_2$	7.3	0.12	[65]
RbCl	7.5	0.17	[17,62]
$KSrPO_4$	7.7	0.14	[66]
BaFBr	7.7	0.12	[67]
KCl	7.7	0.18	[17,62]
$LiSrPO_4$	7.8	0.28	[68]
$LiSrPO_4$	7.8	0.28	[68].
CsCl	7.8	0.28	[17,62]
YPO_4	8.6	0.23	[15,26,28,69]
BaF_2	10.0	0.22	[17]
Cs_2NaYF_6	10.2	0.29	[23]
SrF_2	10.6	0.30	[17]
$LiCaAlF_6$	11.5	0.40	[70]
CaF_2	11.2	0.30	[17]

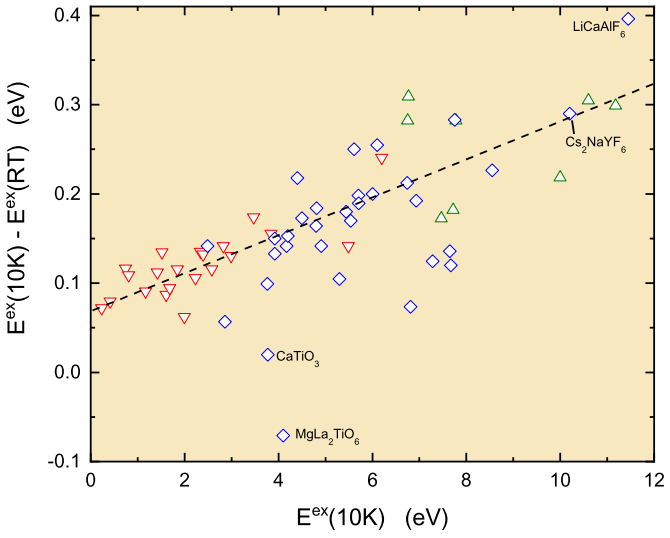

Fig. 3. The decrease of E^{ex} in the temperature range 10 K to RT against the value for E^{ex}(10 K). Each data point is from a different compound. ▽, data on semiconductors from [16]. △, data from alkaline and alkaline earth halides from [17].

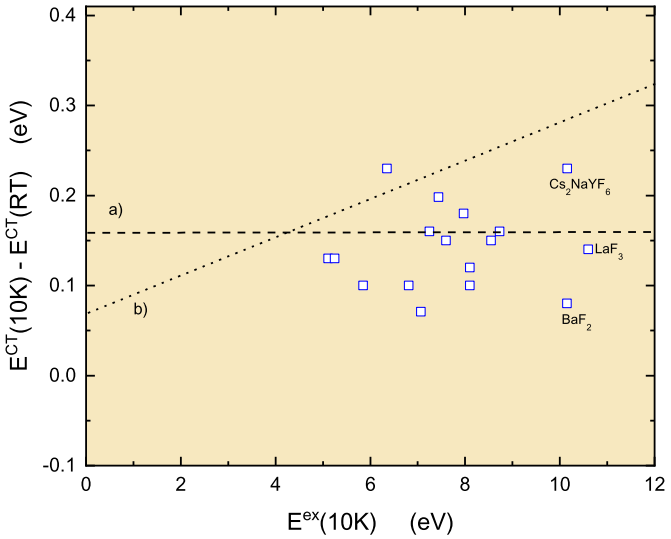

Fig. 4. The decrease of $E^{CT}(Eu^{3+}$ in the temperature range 10 K to RT against the value for E^{ex}(10 K). Each data point is from a different compound. The dashed horizontal line a) shows the compound averaged decrease of 0.16 eV. The dotted line b) represents the typical decrease in E^{ex} between 10 K to RT.

Table 2
The decrease of the energy $E^{CT}(Eu^{3+})$ between 10 K and room temperature together with the value for E^{ex} at 10 K. Energies are in eV.

Compound	E^{ex}(10 K)	E^{CT}(10 K)-E^{CT}(RT)	Ref.
$CaGa_4O_7$	5.1	0.13	[71]
$BaLa_2ZnO_5$	5.3	0.13	[72–74]
Sr_2GeO_4	≈5.6	0.19	[75]
$GdTaO_3$	5.9	0.10	[76–80]
$LiLuGeO_4$	6.4	0.23	[81,82]
Gd_2SiO_5	6.8	0.10	[63]
$LaBO_3$	7.1	0.07	[27,83,84]
$Cs_2NaYCl_6:Sm^{3+}$	7.3	0.16	[85]
$K_3LuSi_2O_7$	7.4	0.20	[86]
$Ca_2Al(AlSiO_7)$	7.6	0.15	[87–91]
$NaYP_2O_7$	8.0	0.18	[92,93]
$GdPO_4$	8.1	0.10	[15,26,94,95]
$LaPO_4$	8.1	0.12	[15,26,94,96]
YPO_4	8.6	0.15	[29,30]
$LuPO_4$	8.7	0.16	[15,30]
BaF_2	10.2	0.08	[97]
Cs_2NaYF_6	10.2	0.23	[23]
LaF_3	10.6	0.14	[98,99]

lowering. On exciting an electron from the valence band to the conduction band not only the energy of the electronic state occupied by the electron will change, i.e., from the top of the VB to the bottom of the CB, but also the energy of the electron-phonon interaction at the VB-top and at the CB-bottom [16,18,24]. Those latter energies will also appear in the measured value for E^{ex}. Many theoretical studies have appeared on the effect of electron-lattice-interaction on the bandgap of materials. The consensus is that it has the same sign as the effect of lattice expansion and its contribution to bandgap lowering is larger than that from lattice expansion [16,24].

The linear expansion coefficient for inorganic compounds like YPO_4, $Y_3Al_5O_{12}$, $LaBO_3$, Y_2O_3 is around 5×10^{-6}/K. If we now assume that screening distance R_{Q+} changes proportionally with lattice expansion, then Eq. (1) predicts that the chemical shift will reduce by around 0.1 meV/K for Eu^{2+} and a factor 3/2 larger for Eu^{3+} when temperature increases. This demonstrates that the CTL at the CB-bottom and of a lanthanide will shift in the same direction with temperature increase but each may shift by a different amount depending on cation charge and radius. The situation is different when the energy difference between the CTL of a cation and an anion is considered where CTLs shift in opposite direction. This is the case for the exciton energy E^{ex} as in Fig. 3. Since the transition from the VB-top to Eu^{3+} is also between an anion and a cation one expects that the CT-energy $E^{CT}(Eu^{3+})$ should like that of E^{ex} decrease with temperature increase. This is already demonstrated with the results for Cs_2NaYF_6 in Fig. 2. Motivated by this, the literature on Eu^{3+} CT data was studied with the aim to retrieve information on E^{CT} at 10 K and at RT. The results are shown in Fig. 4 and tabulated in Table 2. In cases when CT-data were not available at 10 K, values were estimated from extrapolation. That for BaF_2 and $CaGa_4O_7$ were extrapolated from 80 K data, that for Sr_2GeO_4 and $Ca_2Al(AlSiO_7)$ from 20 K and 26 K data. For $K_3LuSi_2O_7$, the 10 K value was extrapolated from 40 C and 300 C data. For Cs_2NaYCl_6, the Eu^{3+} CT-shift is not known and instead that for Sm^{3+} was used.

Fig. 4 shows that E^{CT} like E^{ex} indeed decreases when temperature increases from 10 K to RT. The decrease is on average 0.16 eV which is of comparable magnitude as that for E^{ex} in Fig. 3. Note that data are limited to larger than 5 eV bandgap compounds. Like with E^{ex} again a large compound to compound variation is observed. Other than with E^{ex}, the decrease seems not to scale with the size of E^{ex}.

4. Discussion

The results in Fig. 3 and 4 show that the energy for electron transfer from an anion (the VB-top) to a cation (Eu^{3+} or the CB-bottom) decreases when temperature increases. This demonstrates that when E^{CT} data at RT are combined with E^{ex} data at 10 K to construct a VRBE scheme, errors of magnitude 0.1 to 0.3 eV are unavoidably introduced. Past 10 years such errors were acceptable and usually they still are. However, when one wishes to compare the luminescence quenching energy barrier or the electron or hole trapping depths of lanthanide defects with predictions from a VRBE scheme such errors become of relevance.

The thermal quenching of the 5d-4f emission of lanthanides like Eu^{2+} and Ce^{3+} usually proceeds by thermal ionization of the 5d-electron to the CB [6]. In compounds with a CB-bottom near -3 to -4 eV, the 4f-4f emission from the $^3P_0$ level of Pr^{3+} and from the $^5D_4$ level of Tb^{3+} also often proceeds by thermal ionization from the excited state to the CB [25]. On the other hand, the quenching of the 4f-4f emission from the $^5D_0$ level of Eu^{3+} proceeds by thermal excitation of a hole

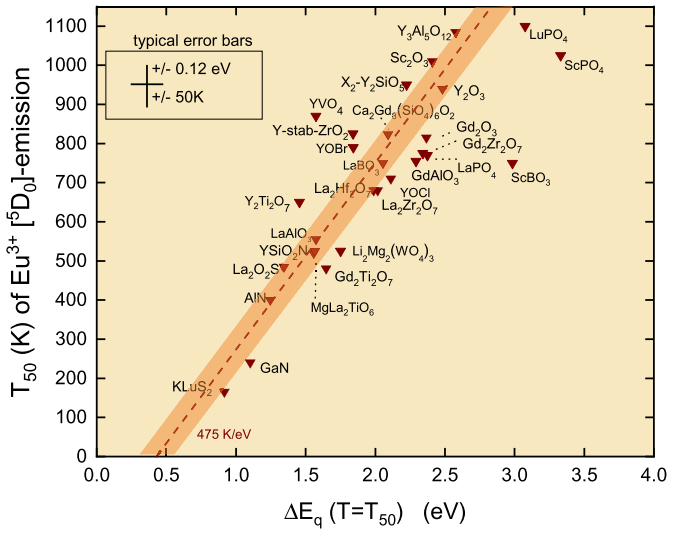

Fig. 5. 50% quenching temperature T_{50} for Eu^{3+} emission from the $^5D_0$ level against the energy difference between the $^5D_0$ hole state and the VB-top. The energy difference was first determined from the room temperature VRBE diagram of the compound, and next a correction to the value at temperature T_{50} was made. The dashed line has the predicted slope of 475 K/eV.

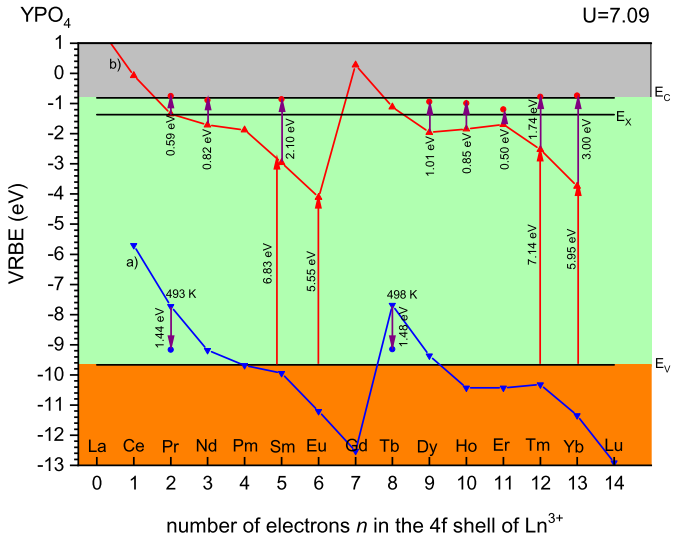

Fig. 6. The room temperature VRBE scheme for the trivalent and divalent $4f^n$ lanthanide ground state levels in YPO_4. Curve a) connects the $Ln^{4+/3+}$ CTL energies, b) connects the $Ln^{3+/2+}$ CTL energies. E_V, E_X, E_C are the VRBE at the valence band top, in the host exciton state, and at the conduction band bottom, respectively. The lengths of the upward pointing arrows starting from E_V correspond with observed energies for electron transfer to trivalent lanthanides. The lengths of upward pointing arrows starting at the $Ln^{3+/2+}$ CTLs correspond with electron trap depths derived from TL-data in [34]. The solid bullet data symbols mark the endpoints. The length of the down pointing arrows starting at the $Pr^{4+/3+}$ and $Tb^{4+/3+}$ CTL with endpoints marked with solid bullet data points correspond with the hole trap depth derived from TL-data in [15].

from Eu^{3+} to the VB-top. The temperature T_{10} or T_{50} where luminescence intensity has dropped by 10% or 50% provides then information on the quenching energy barrier ΔE_q that can be compared with the barrier read from a constructed VRBE diagram. Such analysis was done for all above five lanthanides in Ref. [6] with the aim to validate the VRBE-diagrams. Depending on compound, the quenching temperature may range from 10 K to 1000 K, and over such temperature range one has to take the effect of temperature on CTL values and related quenching energy barrier into account in order to make a proper validation. When dealing with Eu^{2+}, Ce^{3+}, Pr^{3+}, and Tb^{3+} quenching proceeds by a cation (the lanthanide)-to-cation (the conduction band) electron transfer and it was assumed that the CTL of the lanthanide changes with the same sign and the same pace as the CTL at the CB-bottom. The quenching energy barrier is then independent on temperature. On the other hand for Eu^{3+}, quenching of its $^5D_0$ emissions proceeds by hole transfer from Eu^{3+} to the VB-top. Now, we are dealing with a cation to anion transition and the quenching energy barrier is proportional to E^{CT} that does change with temperature as shown in Fig. 4. In [6] the quenching energy barrier for the $^5D_0$ emission at the quenching temperature T_{10} was evaluated as

$$\Delta E_q(T_{10}) = E^{CT} - 5\times 10^{-5} T_{10} E^{ex} - E(^5D_0) \quad (3)$$

where $E(^5D_0)$ is the energy 2.18 eV of the $^5D_0$ state above the ground state, and where a linear dependence with T_{10} and with E^{ex} was assumed. Based on the results in Fig. 4 it is better to use

$$\Delta E_q(T_{50}) = E^{CT}(293K) - \frac{0.16}{283}(T_{50} - 293) - E(^5D_0) \quad (4)$$

where the room temperature CT energy is corrected for the expected lowering at the quenching temperature of T_{50}.

In [6] it was predicted that the quenching temperature T_{10} should change with ΔE_q with a rate of 435 K/eV and data indeed displayed such prediction. However ΔE_q was derived from a VRBE diagram constructed with $E^{ex}(10K)$ and E^{CT} at unspecified temperature together with the correction from Eq. (3). This procedure is not entirely just. We therefore reanalysed the data by deriving the quenching energy barrier from the VRBE diagram constructed with E^{ex} and E^{CT} values both pertaining to RT and using Eq. (4) for temperature correction. Furthermore we used the T_{50} value instead of the T_{10} value. The re-analysed results are shown in Fig. 5.

The dashed line in Fig. 5 has a slope of 475 K/eV as was predicted from the single energy barrier Arrhenius equation in [6]. The intercept at about $\Delta E_{offset} = 0.45 \pm 0.12$ eV has been attributed to 1) the energy involved in lattice relaxation that goes along with a charge carrier transfer in a compound, and 2) the hole at the valence band is stabilized by bonding to the transferred electron [6]. Apart from this offset energy, the data follow the dashed line which demonstrates that the method of VRBE diagram construction is consistent with observed quenching temperatures.

The general idea that the CTL of cations lowers when temperature increases and that the CTL of anions moves up is reflected in the temperature dependence of anion to cation CT-energies like that of E^{ex} and $E^{CT}(Ln^{3+})$. The CTL of two different cations will move in the same direction and that would imply that the energy differences between cation CTLs are expected to be less dependent on temperature. This is the reason that in evaluating the quenching energy barriers for Ce^{3+} and Eu^{2+} 5d-4f emission and 4f-4f emission in Pr^{3+} and Tb^{3+}, a correction for temperature was not made in [6].

In thermoluminescence experiments one probes the release of charge carriers from either electron traps or from hole traps. The release of an electron from a lanthanide to the CB is a cation-to-cation electron transfer and then the e-trap depth will not change much with temperature. On the other hand the release of a hole from a lanthanide to the valence band is a cation to anion hole transfer which then should show a temperature dependence of similar magnitude as observed for E^{ex} and $E^{CT}(Eu^{3+})$. To verify those expectations, this work has re-analysed the results on thermoluminescence studies of lanthanide doped YPO_4. Fig. 6 shows the VRBE scheme that applies to YPO_4 at RT constructed with $E^{ex}(RT) = 8.3$ eV from [26–28], $E^{CT}(Eu^{3+}, RT) = 5.55$ eV from [27,29–31], and $U = 7.09$ eV from [12]. The energy of the charge transfer band at RT for Sm^{3+} [28,29], Tm^{3+} [29,32] and Yb^{3+} [29,33] are illustrated by the drawn vertical arrows starting at E_V. They all end close to the $Ln^{3+/2+}$ CTL-curve constructed with tilt parameter $\alpha(2+) = 0.095$ eV/pm and nephelauxetic parameter $\beta(2+) = 0.94$.

The lengths of the upward pointing arrows in the scheme of Fig. 6 starting at the $Ln^{3+/2+}$ CTL curve b) represent the electron trapping depths as determined by Bos et al. [34] from the thermoluminescence glow peaks with the variable heating rate method. Here Ce^{3+} was used as a deep hole trap and recombination centre. The maxima of the glow peaks spanned a range from 200 K for the release of an electron from Pr^{2+} to 900 K for the release of an electron from Yb^{2+}. Over such 700 K temperature range, we expect the bandgap to decrease by 0.5 to 0.6 eV. Then, the trapping depth for the deep traps by Sm, Tm, Yb should turn out too shallow in a VRBE diagram pertaining to RT as compared to that of shallow traps. However, this is not observed in Fig. 6. This confirms that the CTLs of lanthanides and E_C shift in the same direction when temperature changes and that the e-trap depths remain temperature independent within, say, few 0.1 eV.

The lengths of the downward pointing errors that start at the $Pr^{4+/3+}$ and $Tb^{4+/3+}$ CTLs correspond with hole trap depths derived from the maxima of TL-glow peaks near 493 K and 498 K in [15] recorded at a heating rate of 1 K/s. We are dealing with a hole transfer from a lanthanide to the VB at 200 K above room temperature. Assuming that Eq. (4) for hole release from Eu^{3+} applies also to hole release from Pr^{4+} and Tb^{4+}, the hole trap depth has reduced by 0.12 eV as compared to the depth at RT. However, the trap depths appear about 0.5 eV smaller than in the room temperature VRBE scheme. There is still a difference of 0.38 eV. One may speculate that the hole does not need to be thermally excited into the valence band but instead may form a so-called V_k centre as suggested in [35]. This is a hole bonded between two oxygen ligands with a CTL above the VB-top that may migrate through the material. On the other hand, the 0.35 eV difference is also of the same magnitude as the systematic errors that can be present in VRBE diagram construction.

5. Conclusions

This work has collected data from literature to demonstrate that E^{ex} and related bandgap energy decrease with temperature increase at a rate that appears to grow with the size of E^{ex}. The reduction from 10 K to RT is about 0.1 eV for small band gap semi-conductors and about 0.3 eV for wide band gap fluorides. The energy for electron transfer from the VB-top to Eu^{3+} shows similar decrease with temperature although a dependence on the size of E^{ex} was not found in this work. The finding means that in constructing a VRBE diagram with the lanthanide CTLs one should use experimental parameters E^{ex} and E^{CT} evaluated at the same temperature, preferably at RT. Shifting of CTLs of lanthanides or the VB-top and CB-bottom are caused by thermal lattice expansion and electron-phonon interaction. It is concluded that cation CTLs like that of lanthanides and at the CB-bottom move downwards, although not necessarily in the same pace when temperature increases. The quenching energy barrier of Ce^{3+}(5d), $Pr^{3+}(^3P_0)$, $Tb^{3+}(^5D_4)$, and Eu^{2+}(5d) luminescence is an energy needed for electron transfer from a cation (the lanthanide) to a cation (the CB). The same holds for the energy for electron detrapping from a divalent lanthanide. One then expects that those energies are to first approximation temperature independent. The energy for hole release from a lanthanide to the valence band, or the energy of electron transfer from the VB to Ln^{3+}, or the energy E^{ex} all deal with charge carrier transfer between an anion and a cation. In those cases, a relatively strong temperature dependence is expected and/or observed. The new insights help in improving the accuracy of VRBE diagram construction with the lanthanide CTLs. It also helps in the interpretation of the quenching energy barrier and trapping depths that are derived from experimental data obtained in a wide temperature range from 10 K to 1000 K.

CRediT authorship contribution statement

Pieter Dorenbos: Writing – review & editing, Writing – original draft, Software, Methodology, Investigation, Formal analysis, Conceptualization.

Declaration of competing interest

The authors declare that they have no known competing financial interests or personal relationships that could have appeared to influence the work reported in this paper.

Data availability

No data was used for the research described in the article.

References

[1] A.J.J. Bos, P. Dorenbos, A. Bessiere, B. Viana, Radiat. Meas. 43 (2008) 222.
[2] S.W.S. McKeever, Thermoluminescence of Solids, Cambridge University Press, Cambridge, 1985.
[3] A.J.J. Bos, Nucl. Instrum. Methods Phys. Res. B 184 (2001) 3.
[4] K. van den Eeckhout, P.F. Smet, D. Poelman, Materials 3 (2010) 2536.
[5] Yue Hu, Xiaoxiao li, Xin Wang, Yunqian Li, Tianyi Li, Hongxiang Kang, Hongwu Zhang, Yanmin Yang, Opt. Express 28 (2020) 2649.
[6] P. Dorenbos, J. Mater. Chem. C 11 (2023) 8129.
[7] P. Dorenbos, J. Lumin. 136 (2013) 122.
[8] P. Dorenbos, Phys. Rev. B 85 (2012) 165107.
[9] P. Dorenbos, J. Lumin. 214 (2019) 116536.
[10] P. Dorenbos, J. Lumin. 222 (2020) 117164.
[11] P. Dorenbos, Phys. Rev. B 87 (2013) 035118.
[12] P. Dorenbos, J. Lumin. 135 (2013) 93.
[13] P. Dorenbos, Opt. Mater. 69 (2017) 8.
[14] A. Lecointre, A. Bessiere, A.J.J. Bos, P. Dorenbos, B. Viana, S. Jacquart, J. Phys. Chem. C 115 (2011) 4217.
[15] Tianshuai Lyu, Pieter Dorenbos, J. Mater. Chem. C 6 (2018) 369.
[16] R. Passler, J. Appl. Phys. 89 (2001) 6235.
[17] G.W. Rubloff, Phys. Rev. B 5 (1972) 662.
[18] H.Y. Fan, Phys. Rev. 82 (1951) 900.
[19] Yuhei Shimizu, Kazushige Ueda, J. Lumin. 168 (2015) 14.
[20] Anna Hankin, Franky E. Bedoya-Lora, John C. Alexander, Anna Regoutz, Geoff H. Kelsall, J. Mater. Chem. A 7 (2019) 26162.
[21] R.D. Shannon, Acta Crystallogr., Sect. A Cryst. Phys. Diffr. Theor. Gen. Crystallogr. 32 (1976) 751.
[22] P. Dorenbos, J. Lumin. 267 (2024) 120358.
[23] P.A. Tanner, C.-K. Duan, V.N. Makhov, M. Kirm, N.M. Khaidukov, J. Phys. Condens. Matter 21 (2009) 395504.
[24] R. Passler, J. Appl. Phys. 88 (2000) 2570.
[25] P. Dorenbos, E.G. Rogers, ECS J. Solid State Sci. Technol. 3 (2014) R150.
[26] E. Nakazawa, F. Shiga, J. Lumin. 15 (1977) 255.
[27] A. Mayolet, Etude des processus d'absorption et de transfert d'energie au sein de materiaux inorganiques luminescents dans le domaine UV et VUV, thesis, Universite de Paris XI Orsay, 1995.
[28] B. Moine, S. Hachani, M. Ferid, J. Lumin. 131 (2011) 2110.
[29] E. Nakazawa, J. Lumin. 100 (2002) 89.
[30] V.S. Levushkina, D.A. Spassky, E.M. Aleksanyan, M.G. Brik, M.S. Tretyakova, B.I. Zadneprovski, A.N. Belsky, J. Lumin. 171 (2016) 33.
[31] V.S. Voznyak-Levushkina, A.A. Arapova, D.A. Spassky, I.V. Nikiforov, B.I. Zadneprovski, Phys. Solid State 64 (2022) 567.
[32] Y. Sato, T. Kumagai, S. Okamoto, H. Yamamoto, T. Kunimoto, Jpn. J. Appl. Phys. 42 (2004) 3456.
[33] E. Nakazawa, Chem. Phys. Lett. 56 (1978) 161.
[34] A.J.J. Bos, P. Dorenbos, A.Q. Bessiere, A. Lecointre, M. Bedu, M. Bettinelli, F. Piccinelli, Radiat. Meas. 46 (2011) 1410.
[35] A.H. Krumpel, E. van der Kolk, D. Zeelenberg, A.J.J. Bos, K.W. Kramer, P. Dorenbos, J. Appl. Phys. 104 (2008) 073505.
[36] R. Ahuja, H. Arwin, A. Ferreira da Silva, C. Persson, J.M. Osorio-Guillen, J. Souza de Almeida, C. Moyses Araujo, E. Veje, N. Veissad, C.Y. An, I. Pepe, B. Johansson, J. Appl. Phys. 92 (2002) 7219.
[37] V.F. Machulin, F.V. Motsnyi, O.M. Smolanka, G.S. Svechnikov, E.Yu. Peresh, Low Temp. Phys. 30 (2004) 964.
[38] A.J.J. Bos, R.M. van Duijvenvoorde, E. van der Kolk, W. Drozdowski, P. Dorenbos, J. Lumin. 131 (2011) 1465.
[39] Michele Back, Jumpei Ueda, Jian Xu, Kazuki Asami, Lucia Amidani, Enrico Trave, Setsuhisa Tanabe, J. Phys. Chem. C 123 (2019) 14677.
[40] Yoshiyuki Inaguma, Takeshi Tsuchiya, Yuki Mori, Yuki Imade, Nobuhisa Sato, Tetsuhiro Katsumata, Daisuke Mori, Thermochim. Acta 532 (2012) 168.
[41] A.H. Krumpel, E. van der Kolk, E. Cavalli, P. Boutinaud, M. Bettinelli, P. Dorenbos, J. Phys. Condens. Matter 21 (2009) 115503.
[42] Junbei Wang, Xianju Zhou, Guotao Xiang, Sha Jiang, Li Li, Yongjie Wang, Yanhong Li, Chuan Jinga Lu Yao, Hongmei Yang, Yanhao Huang, Feng Wang, Dalton Trans. 51 (2022) 17224.
[43] A.J.H. Macke, Phys. Status Solidi A 39 (1977) 117.

[44] L.I. Isaenko, I.N. Ogorodnikov, V.A. Pustovarov, A.Yu. Tarasova, V.M. Pashkov, Opt. Mater. 35 (2013) 620.
[45] V.A. Pustovarov, L.N. Ogorodnikov, N.S. Bastrikova, A.A. Smirnov, L.I. Isaenko, A.P. Eliseev, Opt. Spectrosc. 101 (2006) 234.
[46] V. Jary, L. Havlak, J. Barta, E. Mihokova, P. Prusa, M. Nikl, J. Lumin. 147 (2014) 196.
[47] C. Hidaka, T. Takizawa, J. Cryst. Growth 237–239 (2002) 2009.
[48] O.N. Yunakova, V.K. Miloslavsky, Low Temp. Phys. 28 (4) (2002) 284.
[49] M. Fujita, M. Itoh, S. Takagi, T. Shimizu, N. Fujita, Phys. Status Solidi B 243 (2006) 1898.
[50] Xuan Chen, Guangran Zhang, Robert Tomala, Dariusz Hreniak, Yiquan Wu, J. Eur. Ceram. Soc. 42 (2022) 4320.
[51] L.Y. Cai, X.D. Wei, H. Li, Q.L. Liu, J. Lumin. 129 (2009) 165.
[52] M. Raukas, S.A. Basun, W. van Schaik, W.M. Yen, U. Happek, Appl. Phys. Lett. 69 (1996) 3300.
[53] Tianshuai Lyu, Pieter Dorenbos, Laser Photonics Rev. 16 (2022) 2200304.
[54] N. Yamashita, Jpn. J. Appl. Phys. 30 (1991) 1384.
[55] W.J. van Sciver, Phys. Rev. 120 (1960) 1193.
[56] N. Sata, M. Ishigame, S. Shin, Solid State Ion. 86–88 (1996) 629.
[57] R. Kral, V. Babin, E. Mihokova, M. Buryi, V.V. Laguta, K. Nitsch, M. Nikl, J. Phys. Chem. C 121 (2017) 12375.
[58] T. Tomiki, J. Tamashiro, Y. Tanahara, A. Yamada, H. Fukutani, T. Miyahara, H. Kato, S. Shin, M. Ishigame, J. Phys. Soc. Jpn. 55 (1986) 4543.
[59] A.I. Kuznetsov, V.N. Abramov, N.S. Rooze, T.I. Savikhina, JETP Lett. 28 (1978) 602.
[60] H.H. Tippins, J. Phys. Chem. Solids 27 (1966) 1069.
[61] V. Jary, M. Nikl, E. Mihokova, J.A. Mares, P. Prusa, P. Horodysky, W. Chewpraditkul, A. Beitlerova, IEEE Trans. Nucl. Sci. 59 (2012) 2079.
[62] K. Teegarden, G. Baldini, Phys. Rev. B 155 (1967) 896.
[63] Yonghu Chen, Bo Liu, Chaoshu Shi, Guohao Ren, M. Kirm, M. True, S. Vielhauer, G. Zimmerer, J. Phys. Condens. Matter 17 (2005) 1217.
[64] Yong Li, Yan Pan, Hongmei Chen, Ye Tao, Opt. Mater. 50 (2015) 184.
[65] Huihong Lin, Hongbin Liang, Zifeng Tian, Qiang Su, Hanyu Xie, Jinfu Ding, J. Mater. Res. 21 (2006) 864.
[66] Rongfu Zhou, Litian Lin, Chunmeng Liu, Pieter Dorenbos, Ye Tao, Yan Huang, Hongbin Liang, Dalton Trans. 47 (2018) 306.
[67] E. Nicklaus, Phys. Status Solidi A 53 (1979) 217.
[68] Vladimir A. Pustovarov, Konstantin V. Ivanovskikh, Yulya E. Khatchenko, Qiufeng Shi, Marco Bettinelli, Radiat. Meas. 123 (2019) 39.
[69] L. van Pieterson, M.F. Reid, G.W. Burdick, A. Meijerink, Phys. Rev. B 65 (2002) 045114.
[70] H. Takahashi, M. Sakai, S. Ono, N. Sarukura, H. Sato, T. Fukuda, Jpn. J. Appl. Phys. 42 (2003) L660.
[71] M. Puchalska, E. Zych, J. Lumin. 132 (2012) 2879.
[72] M.J.J. Lammers, H. Donker, G. Blasse, Mater. Chem. Phys. 13 (1985) 527.
[73] Chongfeng Guo, Jie Yu, Jung-Hyun Jeong, Zhaoyu Ren, Jintao Bai, Physica B 406 (2011) 916.
[74] D.R. Taikar, C.P. Joshi, S.V. Moharil, P.L. Muthal, S.M. Dhopte, J. Lumin. 132 (2012) 1112.
[75] K. Fiaczyk, E. Zych, RSC Adv. 6 (2016) 91836.
[76] Mu Gu, Lihong Xiao, Xiaolin Liu, Rui Zhang, Bingjie Liu, Xin Xu, J. Alloys Compd. 426 (2006) 390.
[77] Bo Liu, Mu Gu, Zeming Qi, Xiaolin Liu, Shiming Huang, Chen Ni, Phys. Rev. B 76 (2007) 064307.
[78] Bo Li, Zhennan Gu, Jianhua Lin, Mian-Zeng Su, J. Mater. Sci. 35 (2000) 1139.
[79] Bo Liu, Kun Han, Xiaolin Liu, Mu Gu, Shiming Huang, Chen Ni, Zeming Qi, Guobin Zhang, Solid State Commun. 144 (2007) 484.
[80] Bo Liu, Mu Gu, Kun Han, Xiaolin Liu, Kun Han, Shiming Huang, Chem Ni, Guobin Zhang, Zeming Qi, Appl. Phys. Lett. 94 (2009) 061906.
[81] G. Blasse, A. Bril, J. Inorg. Nucl. Chem. 29 (1967) 2231.
[82] T. Lyu, P. Dorenbos, Chem. Mater. 32 (2020) 1192.
[83] V. Jubera, J.P. Chaminade, A. Garcia, F. Guillen, C. Fouassier, J. Lumin. 101 (2003) 1.
[84] M. Tukia, J. Holsa, M. Lastusaari, J. Niittykoski, Opt. Mater. 27 (2005) 1516.
[85] P.A. Tanner, C.-K. Duan, B.-M. Cheng, Spectrosc. Lett. 43 (2010) 432.
[86] Jingyu Feng, Zhiying Wang, Hanyu Xu, Mochen Jia, Yanling Wei, Zuoling Fu, Inorg. Chem. 60 (2021) 19440.
[87] X.H. Chuai, H.J. Zhang, F.Sh. Li, K.Ch. Chou, Opt. Mater. 25 (2003) 301.
[88] Q. Zhang, J. Wang, M. Zhang, W. Ding, Q. Su, Appl. Phys. A 88 (2007) 805.
[89] Haiyan Jiao, Yuhua Wang, Physica B 407 (2012) 2729.
[90] Penghui Yang, Xue Yu, Hongling Yu, Tingming Jiang, Xuhui Xu, Zhengwen Yang, Dacheng Zhou, Zhiguo Song, Yong Yang, Zongyan Zhao, Jianbei Qiu, J. Lumin. 135 (2013) 206.
[91] Litian Lin, Rui Shi, Rongfu Zhou, Qi Peng, Chunmeng Liu, Ye Tao, Yan Huang, Pieter Dorenbos, Hongbin Liang, Inorg. Chem. 56 (2017) 12476.
[92] Suellen Maria Valeriano Novais, Zelia Soares Macedo, Phys. Status Solidi C 10 (2013) 185.
[93] S.M.V. Novais, A. Dobrowolska, A.J.J. Bos, P. Dorenbos, Z.S. Macedo, J. Lumin. 148 (2014) 353.
[94] S. Hachani, B. Moine, A. El-akrmi, M. Ferid, Opt. Mater. 31 (2009) 678.
[95] N. Yaiphaba, R.S. Ningthoujam, N. Shanta Singh, R.K. Vatsa, N. Rajmuhon Singh, J. Lumin. 130 (2010) 174.
[96] M. Chauchard, J.-P. Denis, B. Blanzat, Mater. Res. Bull. 24 (1989) 1303.
[97] E. Radzhabov, A. Nepomnyashchikh, Solid State Commun. 146 (2008) 376.
[98] I. Gerard, J.C. Krupa, E. Simoni, P. Martin, J. Alloys Compd. 207–208 (1994) 120.
[99] A. Mayolet, J.C. Krupa, I. Gerard, P. Martin, Mater. Chem. Phys. 31 (1992) 107.